Molecular Dynamics Simulations of Rhodopsin in Different One-Component Lipid Bilayers

Arnau Cordomí* and Juan J. Perez

Dept d'Enginyeria Química, Technical University of Catalonia (UPC), Diagonal 647, 08028 Barcelona, Spain

Received: January 30, 2007; In Final Form: April 4, 2007

Four 20 ns molecular dynamic simulations of rhodopsin embedded in different one-component lipid bilayers have been carried out to ascertain the importance of membrane lipids on the protein structure. Specifically, dimyristoyl phosphatidylcholine (DMPC), dipalmitoyl phosphatidylcholine (DPPC), palmitoyl oleoyl phosphatidylcholine (POPC), and palmitoyl linoleyl phosphatidylcholine (PLPC) lipid bilayers have been considered for the present work. The results reported here provide information on the hydrophobic matching between the protein and the bilayer and about the differential effects of the protein on the thickness of the different membranes. Furthermore, a careful analysis of the individual protein−lipid interactions permits the identification of residues that exhibit permanent interactions with atoms of the lipid environment that may putatively act as hooks of the protein to the membrane. The analysis of the trajectories also provides information about the effect of the bilayer on the protein structure, including secondary structural elements, salt bridges, and rigid-body motions.

Introduction

The importance of the lipidic membrane in protein function is a topic that has only recently been the focus of attention of the scientific community.[1] The present view of the membrane is based on the fluid mosaic model of Singer−Nicholson[2] where proteins are distributed in regions of biased composition with varying protein environment. In this heterogeneous landscape, lipids are thought to play a strong influence on protein function, and consequently, it is important to understand the protein−lipid interplay in detail.[3] Specifically, the hydrophobic matching between the protein and the membrane has been identified as one of the most critical aspects of this interaction.[4]

Hydrophobic mismatch is defined as the difference between the hydrophobic length of the transmembrane segments of a protein and the hydrophobic width of the surrounding lipid bilayer. Because of the present difficulties associated with experiments involving membranes or membrane proteins, molecular dynamics (MD) simulations represent an excellent tool to provide some insight into the understanding of lipid−protein interactions. In this sense, the study of model transmembrane peptides[5−10] has provided the necessary background for studying proteins. Of special interest is the recent study where the length of a peptide and the lipid hydrophobic thickness have been studied systematically.[5]

Despite the high number of MD simulations on model peptides reported in the literature, simulations involving membrane proteins are still scarce. Within this group of proteins, G-protein coupled receptors (GPCRs) represent the largest family, being encoded by more than 2% of the human genome, and therefore are of substantial scientific interest. GPCRs mediate a major part of transduction signals responding to a diverse range of molecules, including ions, peptides, lipids, biogenic amines, and photons. These proteins play a key role in cell signal transmission and in the regulation of basic physiological processes. Their key physiological function together with their natural abundance makes them suitable targets for therapeutic intervention, accounting for more than 50% of the currently marketed drugs[11] and, therefore, are proteins of enormous pharmacological interest.[12] Despite their important biological function, scarce structural information, necessary to get a better understanding of the structure−function relationships of GPCRs, is currently available because basically of the difficulties associated with the crystallization of membrane proteins.[13] Bovine rhodopsin, a protein involved in the visual signal transduction cascade in vertebrates, is the only GPCR whose 3D structure is currently available at atomic resolution.[14−18] This makes this protein to be a suitable template for modeling studies of other GPCRs. Recently, different groups have reported simulations of rhodopsin in monounsaturated[19−22] and polyunsaturated model bilayers.[23−25] The results of these studies suggest the existence of specific sites on the rhodopsin surface to accommodate polyunsaturated lipids, and furthermore, the weakening of the interhelical packing with the presence of tightly packed lipids has also been reported.[23−25] However, the effect of different lipid bilayers on the structure and function of the protein is not yet clear.

The aim of the present study is to provide some insight into the understanding of the main features of protein−lipid interactions using rhodopsin as a model of GPCRs. For this purpose, a set of molecular dynamics (MD) simulations of rhodoposin embedded in different lipid environments were performed. Specifically, four 10 ns simulations of rhodopsin embedded in one-component lipid bilayers including dimyristoyl phosphatidylcholine (DMPC), dipalmitoyl phosphatidylcholine (DPPC), palmitoyl oleoyl phosphatidylcholine (POPC), and palmitoyl linoleyl phosphatidylcholine (PLPC) were considered for the present work. Figure 1 depicts pictorially the structures of the different lipids selected for the present study. These lipids were selected for being the best characterized experimentally nowadays and because some inferences can be done in regard to the presence of saturated and unsaturated acyl chains and also the effect of different chain lengths. Despite that these lipids are not the major components of the native membranes where

* To whom correspondence should be addressed. Phone: +34 934010810. Fax: +34 934017150. E-mail: arnau.cordomi@upc.edu.

10.1021/jp0707788 CCC: $37.00
Published on Web 05/27/2007

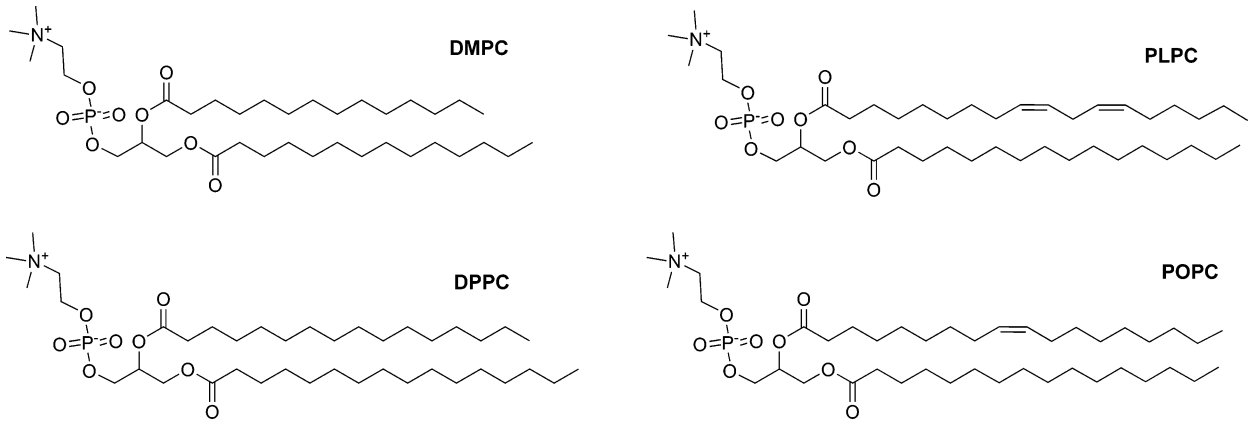

Figure 1. Chemical structures of the different phosphatidylcholine (PC) lipids used in the present work.

rhodopsin is normally found, their choice has special interest since they are some of the most studied lipids and also because force field parameters for them have been widely tested.

Methods

The Rhodopsin Structure. Rhodopsin atomic coordinates were retrieved from the Protein Data Bank[26] (entry 1GZM[17]). In contrast to other published crystal structures,[14−16] this one includes the coordinates of all the amino acids of the intradiscal and cytosolic loops. The atomic coordinates of some missing C-terminal residues were taken from a different source[16] and were adapted by superposition of the α-carbon skeleton of both protein structures. Accordingly, the starting model of the protein contained all N- and C-terminal amino acids, including the N-terminal acetyl group and two palmitoyl chains at the cytoplasmic end that are covalently linked to two consecutive cysteine residues, believed to be important as membrane anchoring points of the protein to the membrane. All amino acids were modeled in the protonation state they would have as free amino acids in water at pH 7 with the exception of D83 and E122, which were treated as protonated and neutral according to experimental evidence.[27] Moreover, H196 was considered charged, as supported by pK_a calculations using the program DaPDS.[28] In these conditions, the protein exhibits a total of 19 positive and 21 negative charges yielding a net charge of −2. This net charge is later compensated in the simulation box by adjusting the balance between sodium and chloride ions to give an electroneutral system, as described in detail later. In addition, 23 crystallographic water molecules, consistent with those found in the crystal structures 1GMZ and 1LH9 of the Protein Data Bank,[16,17] were included in the starting structure.

Box Preparation and Protein Embedding. Four boxes consisting of a lipidic bilayer of 256 molecules of DMPC, DPPC, POPC, or PLPC, respectively, were arranged. For convenience, each system was organized in such a way that the bilayer plane was oriented on the *XY* plane. Introduction of additional water molecules on the systems permits the generation of thick water layers on each side of the bilayer, providing enough space for allocating the hydrophilic parts of the protein. This procedure led to the generation of four boxes of dimensions approximately 8.5 × 8.5 × 10 nm (*XYZ*). Next, sodium chloride was added to the systems to reach a salt concentration of 0.2 M. For this purpose, a different number of water molecules depending on the system were replaced by Na^+ and Cl^- ions one at a time at those positions where the electrostatic potential was more favorable, using the GENION program of GROMACS V3.2.[29,30] The procedure was followed until the desired concentration was reached. Next, each system was equilibrated for 20 ns according the procedure described elsewhere.[31] Finally, rhodopsin was placed in the center of the different boxes and the overlapping molecules were removed, following the procedure described previously.[32] Specifically, all water molecules with oxygen atoms closer than 0.40 nm to a non-hydrogen atom of the protein, as well as all lipid molecules with at least one atom closer than 0.25 nm to a non-hydrogen atom of the protein, were removed. This resulted in four final systems containing 197 lipids and ca. 16 000 water molecules.

Molecular Dynamics Simulations. All computer simulations were performed using a parallel version of the GROMACS 3.2 package.[29,30] Each of the systems was subjected to periodic boundary conditions in the three-coordinate directions. The temperature was kept constant at 323 K for the DPPC system (well above the gel/liquid crystalline phase-transition temperature of 314 K) and at 300 K for the remaining systems using separate thermostats for the protein, water, ions, and lipid molecules.[33] The time constant for the thermostats was set to 0.1 ps except for water, for which a smaller value of 0.01 ps was used. The pressure in the three-coordinate directions was kept at 0.1 MPa by independent Berendsen barostats[33] using a time constant of 1.0 ps. The equations of motion were integrated with the leapfrog algorithm using a time step of 2 fs for the simulations with protein and 4 fs for the rest. All bonds in the protein and lipid molecules were kept frozen using the LINCS algorithm.[34] The bonds and the angles of water molecules were fixed using the analytical SETTLE method. Lennard-Jones (LJ) interactions were computed using a cutoff of 1.0 nm. The electrostatic interactions were treated using the particle mesh Ewald (PME) technique.[35]

The all-atom OPLS force field[36] currently implemented in GROMACS was used for all molecules of the system except for the lipids. In this case, the force field used is based on a parametrization made for DPPC lipids reported in ref 37, which has been shown to reproduce the experimental areas per lipid of pure DPPC in the liquid-crystalline phase.[37−40] For PLPC lipids, the torsion parameters involving the bis-diene moiety were taken from ref 41. Files containing the force field parameters were downloaded from http://moose.bio.ucalgary.ca/. To account for protein−lipid interactions, nonbonded pair interactions were computed as combinations of single atomic LJ parameters. Water molecules were modeled using the TIP3P model.[42] Fractional charges of retinal atoms were taken from quantum chemical calculations[43] and have already been used in other MD simulations of rhodopsin.[21] Fractional atomic

TABLE 1: Hydrophobic Bilayer Thickness for the Systems Studied in the Present Work: Pure Bilayers without Salt (Top), with 0.2 M NaCl (Middle), or with 0.2 M NaCl and Rhodopsin (Bottom)[a]

pure	hydrophobic thickness (nm)		area per lipid (nm)	
DMPC	2.53	±0.02	0.605	±0.005
DPPC	2.82	±0.02	0.634	±0.006
POPC	2.98	±0.02	0.609	±0.004
PLPC	2.82	±0.02	0.647	±0.004
NaCl 0.2 M	hydrophobic thickness (nm)		area per lipid (nm)	
DMPC	2.63	±0.03	0.564	±0.004
DPPC	2.94	±0.03	0.588	±0.006
POPC	3.07	±0.03	0.585	±0.005
PLPC	2.92	±0.03	0.621	±0.005
rhodopsin	hydrophobic thickness (nm)		P−P thickness (nm)	
DMPC	2.65	±0.03	3.75	±0.03
DPPC	2.92	±0.03	4.03	±0.03
POPC	3.02	±0.03	4.12	±0.03
PLPC	2.94	±0.03	4.04	±0.03

[a] For the systems without protein, the areas per lipid are also shown, and for those containing rhodopsin, the phosphate−phosphate (P−P) thickness is displayed instead.

charges for palmitoylated cysteines were derived from electrostatic potential calculations performed at the HF/6-31G* level.

Once the protein was inserted in each lipidic bilayer, the system was energy minimized. Subsequently, each system was subjected to a 0.5 ns MD simulation to allow for the removal of voids present between the protein and the lipids or water. These simulations were performed allowing the three periodic box dimensions to change size according to a pressure of 0.1 MPa in each coordinate direction. The atomic coordinates of the protein were restrained to their crystallographic positions. Next, the restrains were released and the four MD trajectories containing rhodopsin were computed up to 20 ns each. As a reference, eight additional simulations were performed without protein and either with or without ions lasting 20 ns each. For all simulations, coordinates were collected every 10 ps and were stored for further analysis. In all cases, the first 10 ns were considered as equilibration period, and therefore they are not included in the analysis.

Results and Discussion

Effect of the Protein on Lipid Order. The order in a lipid bilayer can be characterized by NMR order parameters, the fraction of trans bonds, from the area per lipid, or through the bilayer thickness. The area per lipid can be directly computed from the total area in systems with no protein embedded. In contrast, this is not straightforward on a system containing a protein because of the bumpy surface exhibited.[32] Therefore, bilayer thickness is preferred as a measure of order for systems containing proteins, measured either from the distance between the two planes formed by the phosphate groups or from the hydrophobic width, that is, the segment of the bilayer corresponding to the acyl chains. In the present work, the hydrophobic width is used since it allows, in the systems with rhodopsin, a direct comparison with the hydrophobic thickness of the protein. Steady values of the bilayer thickness averaged over the last 10 ns for the different simulations are listed in Table 1. The area per lipid for the systems without protein is also given to be used as reference. Average areas of the pure hydrated systems compare well with reported experimental values and with earlier MD simulations of DPPC,[37,38,40,44] DMPC,[38,45] PLPC,[41] and POPC,[46,47] considering the limitations of the lipid parameters available.[48] Furthermore, although comparison with experimental results is not necessarily simple because of the different temperatures used to perform the measurements, the values reported in the present work are within error margins associated to the experimental techniques.[38]

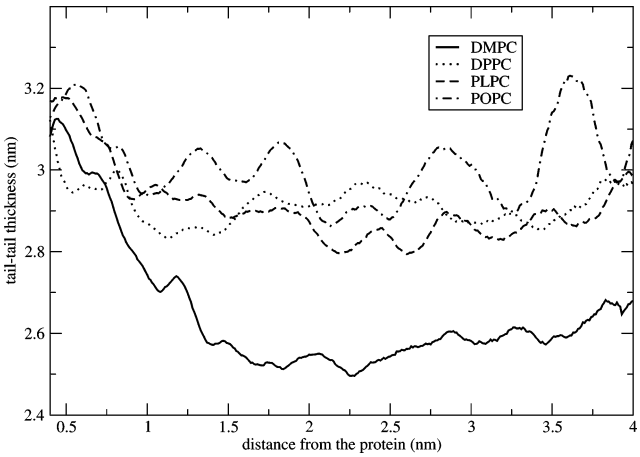

Figure 2. Variation of the bilayer thickness along a radial distance to the protein.

In regard to the effect produced by ions, cations are known to bind to the lipid headgroups promoting lipid order. However, the process of binding requires large simulation times.[49] To use an efficient procedure, we explored the performance of two alternative methods for including ions into the bilayer. Accordingly, we compared a method where ions are placed using a potential-based function versus a random placing. Results suggest that the former procedure provides steady values of the bilayer thickness much faster, being the one used in the present calculations, as explained in Methods. Specifically, the time required for the binding of sodium ions to the lipid headgroups in the present simulations was about 10 ns. Inspection of Table 1 points out that the addition of sodium chloride provides thicker bilayers and, consequently, lower areas per lipid, in agreement with previous results for both pure bilayers[49−51] and bilayers with proteins embedded on them.[32] The decrease in the area per lipid because of the binding of cations to the bilayer is about 7% for DPPC and DMPC and about 4% for POPC and PLPC. These results point out a direct effect of the fatty acid composition on the binding of ions to the lipid headgroups. The decrease is larger in the saturated phospholipids because of a tighter lipid−lipid packing.[52−54]

In regard to the rhodopsin simulations, the results listed in Table 1 indicate that the effect of the protein on the average bilayer thickness is small or negligible for a protein/lipid ratio of about 1/200 as in the systems studied. Similar results were recently obtained in simulations of rhodopsin embedded on a DPPC bilayer under different sampling conditions and handling of the electrostatics.[32] However, in spite of the small average effects produced by the protein on the bilayer thickness, lipids do accommodate to the protein surface in an energetically favorable process known as hydrophobic matching, producing local effects on the bilayer in the neighborhood of the protein. This can be observed from the plot of the bilayer thickness as a function of the distance from the protein, averaged on all the lateral directions, as shown in Figure 2. The differential profile exhibited by each lipid bilayer depends on the difference between the equilibrium lipid bilayer thickness and the hydrophobic thickness of the protein. The four systems studied exhibit a similar thickness of 3.1 nm in the neighborhood of the protein, in good agreement with a previous estimate of 3.0 nm for the

TABLE 2: Average Lennard-Jones (LJ), Coulomb, and Total Interaction Energies between Lipids and the Protein in kJ/mol

	LJ	Coulomb	total
DMPC	−3342	−1145	−4487
DPPC	−3423	−1250	−4673
POPC	−3501	−1136	−4637
PLPC	−3653	−1664	−5317

hydrophobic protein width.[32] Interestingly, this value is close to the hydrophobic thickness of bilayers with a 0.2 M concentration of NaCl (see Table 1) except for DMPC, for which the thickness is significantly smaller than the hydrophobic width of rhodopsin. Therefore, the radial distributions of the bilayer thickness exhibit small variations for DPPC, PLPC, and POPC bilayers, whereas the DMPC system exhibits larger fluctuations basically affecting lipids within a 1.5 nm radius from the protein surface. Furthermore, the profiles displayed in Figure 2 suggest that the thicker region close to the protein is compensated with an increase of the thickness far from the protein, being even lower than the average value without rhodopsin.

Lipid−Protein Interactions. The evolution of both the Coulomb and the Lennard-Jones (LJ) contributions to the lipid−protein interaction energy was investigated along the MD trajectories. In all systems studied, both terms reach a steady value after about 10 ns of simulation. Table 2 lists the values of both contributions for the different systems studied, suggesting a strong interaction between the lipids and the protein in all cases, the magnitude of the LJ contribution being about double the electrostatic one.

LJ interactions account basically for the dispersion contribution to the interaction energy and can be used to evaluate the contact surface, hydrophobic matching, between the protein and the bilayer. The analysis of Table 2 points out that average LJ interaction energies are not the same for the different phospholipids, following the order PLPC > POPC > DPPC > DMPC. Comparison of the LJ interactions for the different systems suggests that their magnitude correlates with the number of carbons on the acyl chain and with the presence of double bonds, which is associated with a better matching of the acyl chains to the protein. More specifically, the smaller LJ contribution exhibited by DMPC in comparison to DPPC (both phospholipids with saturated acyl chains) can be explained as because of the shorter acyl chains of the former, suggesting that they should have to adopt an extended conformation in the vicinity of the protein to account for the differences between their hydrophobic widths and, consequently, impairing an optimal hydrophobic matching. On the other hand, the results of POPC and PLPC suggest that although both have the same number of carbons, the two unsaturations of PLPC provide additional adaptability to the protein when compared to the single one in POPC. These results agree well with the trend observed of an increased bilayer fluidity with a growing number of double bonds of the lipid acyl chains.[53]

Specific hydrophobic lipid−protein interactions have been analyzed along the different trajectories within a radius of 0.4 nm between any hydrophobic heavy atom of rhodopsin and the lipid molecules. Following this approach, about 100−115 residues were identified to exhibit contacts with lipids in at least half of the snapshots analyzed for all systems studied in the present work (Table 3A). This number represents almost one-third of the total number of protein residues, indicating a potential role of lipids in modulating protein structure and function. Obviously, the major part of the interactions observed (90−97% depending on the system) occurs at the lipid tails.

TABLE 3: Summary of Lipid−Protein Hydrophobic Interactions in Each Lipid Bilayer System. (A) Number of Residues Exhibiting Hydrophobic Contacts with the Protein. (B) Number of Residues Grouped per Residue Type

(A) Number of Residues Exhibiting Hydrophobic Contacts with the Protein

	DMPC	DPPC	PLPC	POPC
total residues	102	102	114	110
head	10	10	6	10
tail	92	92	108	100

(B) Number of Residues Grouped Per Residue Type

	DMPC	DPPC	PLPC	POPC	total	%
Ala	6	6	5	4	29	18
Arg	2	2	1	0	7	18
Asn	1	0	0	3	15	7
Asp	0	1	0	1	5	10
Cys	0	1	1	1	10	8
Gln	0	1	1	0	12	4
Glu	0	0	2	2	17	6
Gly	0	0	0	0	23	0
His	2	2	2	3	6	38
Ile	16	16	17	17	22	75
Leu	15	16	17	16	28	57
Lys	1	0	1	0	11	5
Met	7	6	8	8	16	45
Phe	19	19	20	19	31	62
Pro	4	4	6	5	20	24
Ser	1	0	2	1	15	7
Thr	3	2	3	2	27	9
Trp	3	4	4	4	5	75
Tyr	9	9	8	9	18	49
Val	13	13	16	15	31	46
total	102	102	114	110	348	31

This is the case of the residues located on the transmembrane (TM) regions. The remaining interactions involve the lipid-head methyl groups with helix ends or with the loops, which are rich in aromatic residues. Regarding the type of amino acids involved (Table 3B), phenylalanine, leucine, isoleucine, and valine—an aromatic and the most hydrophobic/aliphatic residues—exhibit the largest number of contacts. A second group of amino acids following in importance includes tyrosine and aliphatic residues with shorter side chains like methionine and alanine.

In regard to lipid−protein electrostatic interactions, differences in the energies are observed within the systems studied, despite sharing the same lipid headgroup (see Table 2). This suggests that there is a connection between the hydrophobic matching and the optimization of the electrostatic interactions. Specifically, all systems exhibit average values of about −1200 kJ/mol except PLPC that yields an interaction energy close to −1700 kJ/mol. To understand the source of the Coulomb interactions between the protein and the phospholipids, a careful study of the hydrogen bonds created and broken along the MD trajectory was carried out. Accordingly, two different cutoffs of 0.25 and 0.40 nm were considered to identify direct and water-mediated hydrogen bonds, respectively, involving protein side chain donors and lipid oxygens acting as acceptors. Figure 3 displays residues identified to be involved in more than 5% of the trajectory in direct hydrogen bonds with the lipid molecules or more than 10% of the trajectory in water-mediated hydrogen bonds. The results indicate that the total number of long-time protein−lipid hydrogen bonds depends on the bilayer and ranges from 12 to 21 for the direct and between 21 and 29 when adding the direct plus water mediated ones. Interestingly, an analysis of the figure shows that there are a few residues that are found in all the systems studied and that can be considered as anchoring points of the protein to the lipid bilayer,

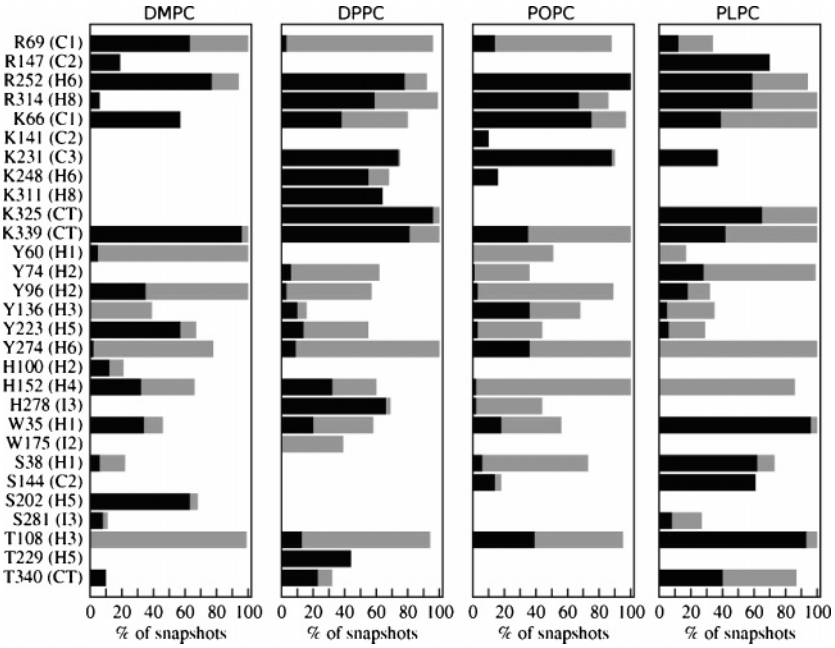

Figure 3. Residues involved in lipid−protein interactions. Only interactions present at least in 10% of the snapshots using a cutoff of 0.40 nm are considered. The location within the protein motifs is indicated in brackets. For each residue, the total bar lengths indicate the percentage of snapshots where the interaction exists. The black and the gray portions of each bar represent the preferences of residues for the phosphate or the carbonyl oxygens, respectively.

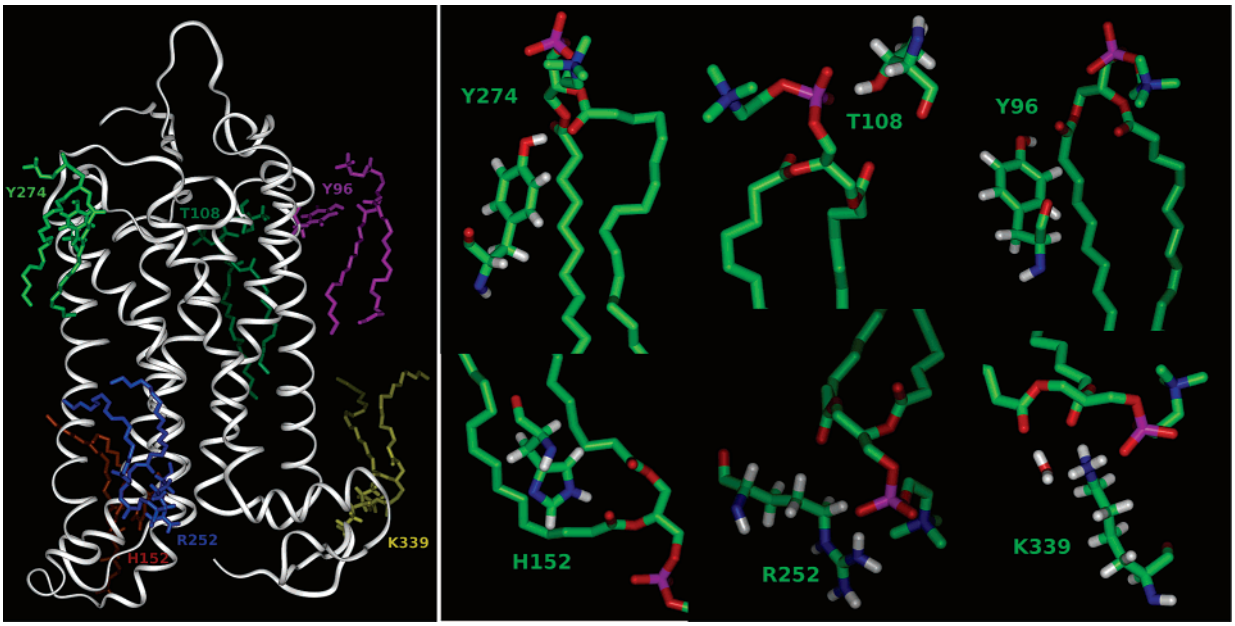

Figure 4. Typical protein−lipid electrostatic interactions involving residues found in common in the four systems to interact with lipids in more than half of each trajectory. The left panel displays the side chain/lipid complexes extracted from representative snapshots of the four simulations superposed to the average protein Cα trace corresponding to the DMPC system. The right one displays a closer view of these interactions, with atoms colored by atom type. The structures displayed for Y274, Y96, and H152 show examples of interactions with the lipid carbonyl oxygens; those of T108 and R252 show interactions with the lipid phosphate oxygens; finally, K339 shows an example of simultaneous interactions with both the lipid carbonyl and phosphate oxygens, including an interaction mediated by a water molecule.

although there is a majority that are only involved in specific systems. According to Figure 3, residues R252, K339, Y96, Y274, H152, and T108 are found in common in the four simulations to be involved in hydrogen bonds with lipid molecules in more than half of each trajectory. A model displaying the location of these residues together with representative interactions with the lipid molecules is shown in Figure 4, where lipid coordinates have been taken from selected snapshots of the four simulations. Additionally, residues K66, R69, Y136, Y223, and W35 participate also in hydrogen bonds with lipid molecules in all systems, though to a lower extent. K339, identified to be present in more than 90% of the four trajectories analyzed, has already been reported to be particularly relevant in both experimental reports[55] and in MD simulations.[19] Most of these critical hydrogen bond interactions (see Figure 3) involve contacts between lipid oxygens and either basic amino acids, lysine and arginine, or polar aromatic ones—tyrosine, histidine, and tryptophan. The short-chain amino acids having hydroxyl groups, serine and threonine, and residues interacting through the backbone nitrogen follow in importance. Examples

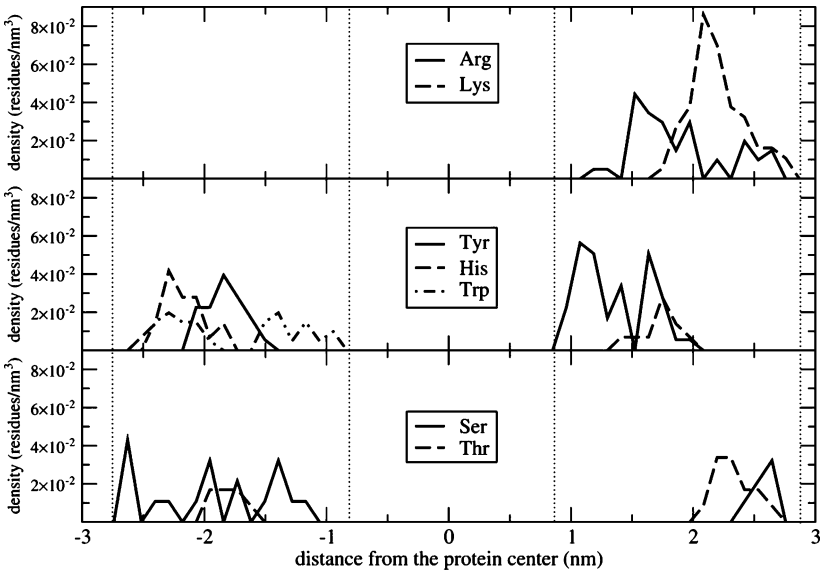

Figure 5. Partial number densities of the residues interacting with lipid oxygens normalized to the number of atoms per residue.

of these interactions between the polar protein side chains and the lipid oxygens can be found in Figure 4.

The preference of each residue for phosphate or alkyl carbonyl oxygens was analyzed. The results were compared with those obtained in both recent MD simulations and experiments on model peptides and proteins.[56−60] The present results show that basic amino acids exhibit a clear preference for phosphate oxygens, in agreement with those results. Polar aromatic residues exhibit also specific preferences: tyrosine exhibits a preference to interact with alkyl carbonyl oxygens, in agreement with other recent reports,[61,62] whereas histidine and tryptophan can be seen to interact indistinctly with both types of oxygens. These differences seem to arise from the location of the hydrogen bond donor, out of the ring in the former. Serine and threonine residues, as well as those residues interacting with the lipids through the backbone nitrogen, do not show a preference for any lipid oxygen type. This is reasonable because of their short side chains, which force them to form hydrogen bonds with the closest lipid oxygens available, independently of their nature. The fact that none of the hydrogen bond interactions through backbone nitrogens are found in common among the different systems suggests that they are formed just to reinforce other existing neighboring hydrogen bonds.

The preference observed by the different amino acids to interact with either the phosphate or carbonyl lipid oxygens suggests that they may not be randomly distributed in the rhodopsin structure. Indeed, Figure 5 depicts pictorially the distribution per amino acid of the different residues shown in Figure 3 along the direction perpendicular to the bilayer normal. As can be seen, the amino acids are grouped around two areas at both sides of the protein located about 2 nm from the protein core, covering a region of approximately 2 nm each. Interestingly, the distribution of these amino acids at both sides of rhodopsin is asymmetric. Thus, arginine and lysine residues are only found on the cytoplasmic side, like most of the tyrosine residues. However, the former are located in the most external segment according to their preference to interact with the phosphate oxygens, whereas the latter are never located at the most external part of the density profiles, according to their preferences for the carbonyl oxygens. Moreover, whereas the majority of arginine and lysine residues interacting with lipids in rhodopsin are located on loops, all tyrosine residues are found in the TM helices, even in quite internal positions such as in the case of Y223. The amphiphilic character of the tyrosine residues together with the long distance between the α-carbon and the hydroxyl group (typically 0.65 nm) is responsible of this behavior. Regarding the tryptophan, histidine, serine, and threonine side chains involved in specific interactions with the lipids, their number is too small to extract general conclusions to be extrapolated to other GPCRs, although the corresponding analysis is performed in detail below. All histidine residues are found closer to the two ends of the protein than tyrosine, probably because of the lower distance between the α-carbon and the ring nitrogen atoms (about 0.45 nm). Despite that tryptophan residues are often present at the TM ends in membrane proteins, only two of them exhibit protein−lipid interactions in rhodopsin, and both are located in the intradiscal side, exhibiting similar relative positions as those found for histidine or tyrosine. Finally, regarding nonaromatic residues with hydroxyl groups, the only serine and the two threonine residues present in the cytoplasmic side are located in the most external part of the density profile. In contrast, in the intradiscal side, the only threonine residue found is located in the central part of the diagram, whereas the three serine amino acids are widely distributed over the whole area.

These results suggest that the distribution of the amino acids involved in interactions with the lipid oxygens is indeed optimized according to each residue type, indicating that rhodopsin sequence, and probably that of other membrane proteins, may have evolved to make use of these preferred locations. These results also show that the majority of the hydrogen bonds identified between rhodopsin and the lipid oxygens lies in the cytoplasmic side. Moreover, considering that the activation of GPCRs involves the cytoplasmic loops bound to the G-proteins, the present results suggest that the existence of specific lipid−protein hydrogen bonds can be important to modulate loop conformations and, in turn, for the signal transduction process.

For all systems studied, most of the aromatic residues—tyrosine, histidine, and tryptophan—involved in hydrophobic interactions participate also in hydrogen bonds with the lipid oxygens. This finding agrees with recent results regarding the importance of this type of residues as anchoring hooks to the lipid bilayer.[58,60] Previous studies of membrane proteins proposed that lysine and arginine residues may "snorkel" to the

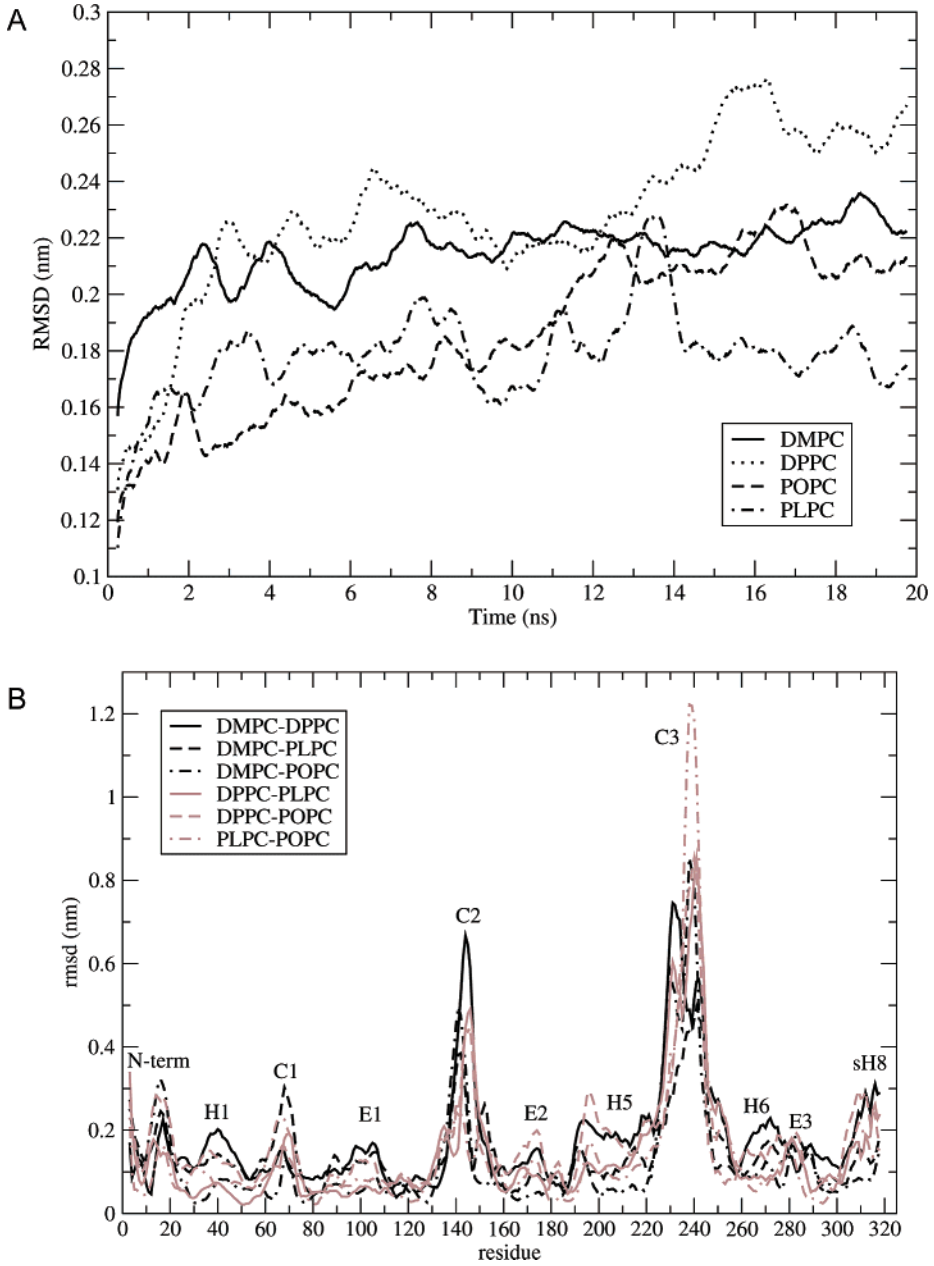

Figure 6. (A) Evolution of the root-mean-square deviations (rmsd) of the α-carbon atom subset from the starting structure excluding the C-terminal segment (see text). Lines are drawn using a running average over 0.5 ns. (B) Rmsd per residue between average structures obtained from the last 5 ns of each simulation.

lipid headgroups through charge−charge interactions with lipid head oxygens and hydrophobic interactions between their side chains and the lipid acyl chains. However, the number of hydrophobic interactions involving these residues in our study is small, suggesting a specific distribution of these residues in the direction of the bilayer normal either for rhodopsin or for GPCRs in general.

Protein Structure. Time evolution of the protein structure was monitored through the root-mean-square deviation (rmsd) from the starting structure measured on the Cα skeleton. Because of the flexibility of the C-terminus, and since it is sensitive to the bilayer thickness close to the protein,[32] the segment up to the palmitoylated cysteines was excluded from the calculations. The results are depicted pictorially in Figure 5 for the different systems studied. The different rmsd values range between 0.16 and 0.28 nm and can be considered as small taking into account the uncertainties of the X-ray structure used as starting point and the length of the simulations. However, the fact that the rmsd values differ from one system to another suggests that lipids stabilize the starting structure in different manners or that each lipid type can modulate the protein structure in a different way.

Inspection of Figure 6A indicates that the rmsd decreases inversely to the number of insaturations with the lipid molecules. This agrees with the observation that the number of double bonds of the acyl chains increases the fluidity of the bilayer and helps in maintaining the crystal structure.[53] The largest rmsd values are found for the DPPC system, followed by the other unsaturated system, the DMPC one. In the latter case, the lower rmsd may be due to the requirement to keep an extended conformation to maximize the hydrophobic matching, which in turn reduces the flexibility of the hydrophobic chains around the protein. These results suggest that the complementarity between the bilayer thickness and the protein hydrophobic width, together with the intrinsic conformational profile of the lipid chains, affects protein structure.

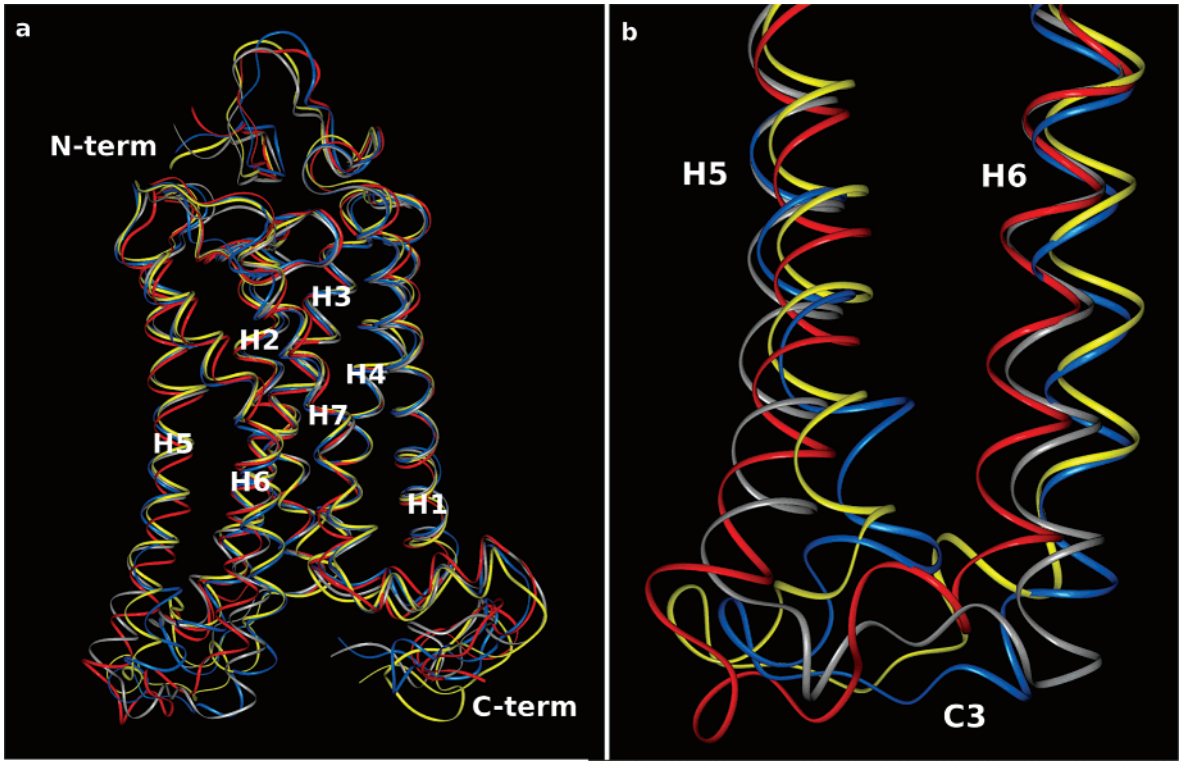

Figure 7. Trace superposition of the average protein structures computed from the last 10 ns of each simulation: (a) the α-carbons of the whole protein and (b) only the cytoplasmatic ends of helices 5 and 6. The structures computed from each system are shown in different colors: DMPC (blue), DPPC (red), POPC (brown), and PLPC (yellow).

To assess the regions of the protein with a larger deviation from the initial structure, averages structures from the last 5 ns of each simulation have been produced. A trace superposition of these structures is shown in Figure 7a. Inspection of the figure reveals that the largest deviations, though small, are located in the cytoplasmatic half of the protein, mainly in regions out of the TM segments, but also in the cytoplasmic halves of helices 5 and 6 (Figure 7b). On the contrary, the intradiscal side does not change much except in the N-terminus, where minor differences are observed. For a better characterization, the rmsd per residue has been computed and the results are displayed pictorially in Figure 6B. Inspection of this plot clearly highlights that the deviations are small in all cases except for the solvent exposed parts, that is, loops and terminal segments, but mainly on the second and third cytoplasmic loops. In the latter case, the deviations extend to the cytoplasmatic halves of helices 5 and 6 in agreement with Figure 7b. However, despite being known that rhodopsin loops are not properly sampled in simulations of the length of the present one,[63,64] the results suggest the active role of the lipid molecules in the modulation of these loops, which are involved in the interaction with G-proteins. The remaining segments of the protein exhibit rmsd values around 0.1 nm.

Transmembrane Helix Lengths and Secondary Structure. The effects of the membrane structure on the secondary structure of rhodopsin were analyzed using the procedure described elsewhere.[32] MD simulations allow the consideration of dynamic effects present in the secondary structure that cannot be observed in the crystals. Specifically, the evolution of the intrahelical hydrogen bonds among residues located on the TM helices was monitored, and the predominant interaction for each pair of residues was identified (Table 4). This analysis provides consensus boundaries for the TM helices, which is of great importance taking into account the existing discrepancies among the available crystallographic structures of rhodopsin. Specifically, the largest ones are located on the cytoplasmic segments of helices 5 and 6 possibly because of crystal packing artifacts. As shown in Table 5, the consensus TM segments obtained are as follows: H1: 34−65; H2: 72−101; H3: 107−140; H4: 149−169; H5: 201−233; H6: 244−279; H7: 288−309; and sH8: 309−320, where H1−H7 are helices 1−7 and sH8 is the short helix 8 perpendicular to the bundle. Interestingly, the most significant discrepancies with the crystal structures are located on the cytoplasmic side of helices 4−7.

The results, shown in Table 4, highlight the existence discontinuities in the TM helices associated in most cases to the localization of helix kinks reported for the crystal structure.[17] The kinks are known to improve the packing of the TM helices but also to play an important role during the activation process. Some of these kinks are proline-induced, with most of the prolines being conserved through the rhodopsin-like family of receptors: P170 and P171 in helix 4, P215 in helix 5, P267 in helix 6, and P302 in helix7. Moreover, additional discontinuities are created, or previously existing ones are reinforced, with the existence of other types of helix-disrupting residues such as glycines or residues that are able to form additional hydrogen bonds competing with the $i - i + 4$ interactions that from an ideal α-helix such as threonine, serine, and histidine.[65]

Specifically, the only discontinuity found in helix 1 is caused by the nonconserved P53 and is reinforced with the neighboring G51. In helix 2, the main distortion appears close to two consecutive glycine residues (G89−90) which favor that three neighboring threonine residues (T92−94) can participate in backbone hydrogen bonds.[17] In helix 3, the discontinuity is found also at two consecutive glycine residues (G120−121) that are close to E113, the counterion of the protonated Schiff base. The conserved P170 and P171 induce discontinuities at the cytoplasmatic end of helix 4, and therefore, they are not considered as part of this helix according to the previous criteria. The main discontinuities in helix 5 are associated to the

TABLE 4: Analysis of Intrahelical Hydrogen Bonding[a]

	H1	FEAPQYYLAE 34 **PWQFSMLAAYMFLLIMLGFPINFLTLYVTVQH** 65 KK
DMPC		----3----3 AAAAAAAAAAAAAAA--AAAAAAAAAAA---3 3-
DPPC		----3----3 AAAAAAAAA3AAAAA--AAAAAAAAAAA---3 --
PLPC		----3----3 3AAAAAAAAAAAAAAA--AAAAAAAAAAA---3 --
POPC		----3----3 3AAAAAAAAAAAAAAA--AAAAAAAAAAA---3 --

	H2	LRTP 72 **LNYILLNLAVADLFMVFGGFTTTLYTSLHG** 101 YF
DMPC		--33 3AAAAAAAAAAAAAAA--3AAAAAAA---- -3
DPPC		--33 3AAAAAAAAAAAAAAA--3AAAAAAA3--- -3
PLPC		--33 AA3AAAAAAA33A-PA--3AAAAAAA3--- -3
POPC		--33 AAAAAAAAAA33AAAA--3AAAAAAA3--- -3

	H3	VFG 107 **PTGCNLEGFFATLGGEIALWSLVVLAIERYVVVC** 140 KPMS
DMPC		--3 3AAAAAAAAAAAA-AAAA3AAAAA3AA3AA---- --3-
DPPC		--3 AAAAAAAAAAAAA-AAA333AAAA3A3-3A---- --3-
PLPC		--3 AAAA-AAAAAAAA-AAAA33AAAA33A--AA--- --3-
POPC		--3 AAAAAAAAAAAAA-AAAA333AAA33333A---- ----

	H4	NFRF 149 **GENHAIMGVAFTWVMALACAA** 169 PPLVGWSRYI
DMPC		---- AAAAAAA33AAAAAAA---3 A3--------
DPPC		---- A-33AAA333AAAA3AA---3 A---------
PLPC		---- A-3AAA-333AAAA3AA---3 A3--------
POPC		---- AAAAAAAA3AAAAA3AA---3 A---------

	H5	YYTPHEETNN 201 **ESFVIYMFVVHFIIPLIVIFFCYGQLVFTVKEA** 233 AAQQQ
DMPC		----33--33 3AAAAAAPP--AA3AAAAA33---3--PP-3-A A3---
DPPC		----33--33 AAAAAAAPP--A3333AAAAAA-AA--3A---A A3---
PLPC		----33--3A AAAAAAAPP--AAAAAAAAAAAA-33A3A---3 33---
POPC		----33---3 AAAAAAAPP--A33AAAAAAAAAAAAAAAA3-A A---3

	H6	ESATT 244 **QKAEKEVTRMVIIMVIAFLICWLPYAGVAFYIFTHQ** 279 GSDF
DMPC		-3A3A A-33A333AAAAAAAA-3A--AAAAAAAAA3--3- ----
DPPC		-3--- AAAAAA-3AAAAAAAA--A--AAAAAAAAAA--3- ----
PLPC		-3AA- A--3A333AAAAAAAA--3--AAAAAAAAAA--3- ----
POPC		--333 AA3AAA33AAAAA3AA-3A--AAAAAA3AAAA--3- ----

	H7	GPIF 288 **MTIPAFFAKTSAVYNPVIYIM** 308
DMPC		---3 AAAA3---3A--333AAA---
DPPC		---3 AAAA3---3A--3-3AAA---
PLPC		3A3- AAAA3---3A--333AAA---
POPC		AA33 AAAA3---3A--333AAA---

	sH8	309 **MNKQFRNCMVTT** 320 LCCGKNPLGD
DMPC		AAAA-3AA3--- ----------
DPPC		AAAAAAAA3--- ---------33
PLPC		AAAAA-AA3--- ----------
POPC		AAAA-33A---- ----------

[a] 3, A, and P account for $i - i + 3$, $i - i + 4$, and $i - i + 5$ interactions, respectively. The fragments in bold show the consensus transmembrane segments including residues up to $i + 4$.

conserved P215 and also to H211. The conserved P267 together with the strongly retinal-coupled[66] W265 are responsible for the pronounced kink at the center of helix 6. Finally, T297 and S298, on one hand, and the conserved P303, on the other, induce the two discontinuities in helix 7. Interestingly, in all systems, helix 7 is by far the least ideal α-helix, with only eight pairs of $i - i + 4$ interactions among the 18 pairs. Moreover, this helix exhibits a strong propensity to form $i - i + 3$ interactions, with five pairs on average.

Some TM segments exhibit additional irregularities on relatively unstructured regions when comparing to an ideal α-helix which are lipid type dependent, affecting preferably the cytoplasmic sides of the helices. Accordingly, we observe alterations in some residues because of either the absence of intrahelical hydrogen bonds or the appearance of $i - i + 3$ interactions as the predominant ones which differ from one simulation to another. In helix 3, it involves a region close to W126 and another one around amino acids E134, R135, and Y136, which are part of the E(D)RY motif critical for activation. Interestingly, residues of the ERY motif lie at the cytoplasmic end of this helix, exhibiting hydrogen bonds with the preceding $i - 3$ or $i - 4$ residues in all cases and with the following $i + 3$ and $i + 4$ only for some systems. A central region of helix 4 around G149, N151, H152, and G156 is also affected. Moreover, the differences are more important when looking at the cytoplasmic sides of both helices 5 and 6, consistent with the differences between the crystal structures available. The present results show that these regions are dynamic and that they alternate between $i - i + 4$, $i - i + 3$, $i - i + 5$, and no intrahelix interactions. Specifically, the region with irregularities in helix 5 is around G224 and T229 and in helix 6 around E247, which interacts with the R135 of the E(D)RY motif. Interestingly, within the segment corresponding to residues 244−252, there are no helix-disrupting amino acids, pointing to the existence of five charged residues on this segment (see Table 4) as responsible for the alterations on the secondary structure.

Another important feature of the analysis reported in Table 4 is the existence of structured segments at the boundary between the TM segments and loops. This can be clearly

TABLE 5: Percentage of Occurrence of Salt Bridges between Rhodopsin Residues in the Different Bilayer Systems Using a Cutoff of 0.4 nm

− residue		+ residue		DMPC	DPPC	PLPC	POPC
E5	NT	R177	I2	0	24	64	13
E25	NT	R21	NT	15	100	75	51
E113	H3	K296	H7	100	100	100	100
E134	H3	R135	H3	99	99	100	98
E150	H4	R147	C2	0	100	100	98
D190	I2	R177	I2	100	100	100	100
E232	C3	K231	C3	20	0	0	29
E232	C3	K245	H6	0	0	98	0
E239	C3	K248	H6	0	0	0	95
E239	C3	K141	C2	93	0	99	0
E247	H6	R135	H3	94	100	86	68
E249	H6	R252	H6	100	100	99	97
D330	CT	R314	H8	59	0	0	0
D330	CT	K311	H8	0	0	59	0
D331	CT	K67	C1	0	0	94	0
D331	CT	K311	H8	26	99	2	100
D331	CT	R314	H8	46	0	0	0
E332	CT	K311	H8	0	2	0	93
E341	CT	K325	CT	40	1	0	0
A348	CT	R147	C2	100	78	1	93

observed between residues 169−171 in helix 4 for all lipid types. The results indicate that the existence of these consecutive turns at these positions complements the short length of this helix, significantly smaller than the other helices and shorter than the one provided by the static crystal structures. Similar features can be observed in the regions of the third cytoplasmic loop closer to the cytoplasmic ends of helices 5 and 6, but the differences from one lipid type to another become larger.

In summary, the stable parts of the α-helices over the trajectory are not affected by the lipid type. On the contrary, those regions where the helices are less stable, that is, those with higher propensity to form $i - i + 3$, and to a less extent $i - i + 5$, or even to lose the intrahelical backbone hydrogen bond, are more sensitive to the lipid type and particularly to the specific conformations adopted by the lipid acyl chains.

Salt Bridges within Rhodopsin. The evolution of all feasible salt bridges in rhodopsin was monitored using a cutoff of 0.3 nm after identification of all possible polar residues involved. The results shown in Table 5 indicate that only 5 out of 20 pairs exhibit significant interactions independently of the bilayer type: E113-K297, E134-R135, D90-R177, E247-R135, and E249-R252. Interestingly, all these residues lie in the TM segments except the pair D90-R177, which involves two residues at the second intradiscal loop. Furthermore, most of these interactions are structurally important: E113-K297 involves the protonated Schiff base and its counterion, and both E134-R135 and E247-R135 are known to play a key role in the activation of most GPCRs.[67] It is important to outline that the latter interaction exhibits different residence times within each system, suggesting the role of lipids in modulating rhodopsin structure and activation.

From all the interactions listed in Table 5, only three of them involve the intradiscal loops or the N-terminus. In contrast, the cytoplasmic loops together with the C-terminus are involved in 13 salt bridges. This asymmetry explains the larger root-mean-square fluctuations (rmsf) reported previously for the cytoplasmic side of rhodopsin than for the intradiscal.[20,32] Moreover, the existence or not of interactions involving residues either at the second or the third cytoplasmic loops or at the C-terminal, the most flexible parts of the protein, has effects on the rmsf (data not shown). This has important implications since the regions that exhibit the largest rmsd between the average structures with the different systems (see Figure 5) correspond also to those with the largest rmsf. Specifically, the absence of the interaction between the charged C-terminal residue A348 and R147 at the second cytoplasmic loop in the PLPC simulation seems responsible for the larger deviations found in this region for this system. Similarly, the lower persistence of contacts between E247 at H6 and R135 at H3 in POPC may be responsible of the larger rmsf at the third cytoplasmic loop observed in simulation. Despite that the interactions involving residues at the C-terminus are not shared within the different systems, important interactions between the short helix 8 and the C-terminus can be observed in all cases. Specifically, the interactions involve two proximal positively charged residues in helix 8 (K311 and R314) and three consecutive negatively charged residues at the C-terminus (D330, D331, and E332). Therefore, the possible combinations of ionic pairs available allow the existence of multiple distinct conformations which can have functional implications. Similarly, the rmsd on the second cytoplasmic loop is smaller in the simulations exhibiting the interaction E150−R147. Moreover, the existence of an ionic lock between the second and the third cytoplasmic loops seems to retain the conformation of the former.

The analysis of the salt bridges in rhodopsin indicates that those observed in the cytoplasmic loops and the C-terminal segment are sensitive to the specific lipid bilayer, whereas the salt bridges buried in the protein core remain relatively unaltered. Moreover, the results suggest a possible role of lipids in the

TABLE 6: Tilt Angles for the Protein as a Whole and Tilt and Kink Angles for Each Specific Helix (H1−H7) in the Simulations and in the Crystal Structure 1GZM[a]

tilts	H1 34−65	H2 72−101	H3 107−140	H4 149−169	H5 201−233	H6 244−279	H7 288−309	overall bundle
1GZM	25	19	24	12	23	16	20	
DMPC	21	17	21	14	20	13	19	8
DPPC	24	21	22	9	24	15	21	8
POPC	24	19	22	12	23	16	21	7
PLPC	22	19	22	13	23	13	20	16

kinks	H1 34−53−65	H2 72−92−101	H3 107−115−140	H4 149−160−169	H5 201−214−233	H6 244−264−279	H7 288−296−309
kinks	15	25	8	6	11	34	29
DMPC	17	11	7	6	11	39	23
DPPC	19	10	15	6	25	48	30
POPC	19	11	10	6	22	44	26
PLPC	16	14	11	7	17	47	28

[a] Reference 17. The intervals indicate the residues considered.

modulation of the electrostatic lock at the cytoplasmic side of helices 3 and 6. The results support the idea that the different lipid−protein interactions provided by each bilayer type can modulate protein structure and function.

Protein Rigid-Body Motions. There is evidence that lipid composition and specifically the bilayer thickness can modulate the rigid-body orientation of the protein as a whole as well as the individual helices (or parts of it) relative to the direction perpendicular to the bilayer. Moreover, in lipid bilayers with a thickness shorter than the hydrophobic width of the protein, tilt is known to be a mechanism to improve the hydrophobic matching.[5,68−70] To compare the effect of the different lipidic environments on the rigid-body motions of rhodopsin, the evolution of the protein tilt from the direction perpendicular to the bilayer has been computed for all the simulations. Specifically, the overall protein tilt was measured from the vector obtained by averaging the positions of the last eight residues of each TM helix on the two sides of the protein. The average tilt values shown in Table 6 range between 7 and 16°. These results indicate that there is a small change in the orientation as a consequence of the different lipidic environments. The largest tilt is observed for the PLPC system, consistent with the largest lipid−protein interaction energies described above.

The tilt angles for each individual helix were calculated from the vectors obtained considering the positions of the last eight residues at each TM helix end and were measured from the vector resulting after averaging the seven helices. The results, shown in Table 6, reveal small or negligible differences both between the average values in each simulation and when compared with the angles obtained in the crystal structure.[17] Differences are always below 5°, indicating that lipids almost do not affect the orientation of the helices. Additionally, the kink angles were computed for each helix by defining two vectors analogously to tilts, on the basis of the discontinuities in the secondary structure described below, considering three residues at each helix end and three residues centered at the main discontinuity. The results indicate that some kinks are sensitive to the lipidic environment. Specifically, in all simulations, helices 2 and 6 exhibit differences when compared to the crystal structure (up to 15°), suggesting that the conditions required for the crystallization may affect the native conformation of these kinks. Moreover, despite that in some simulations helices 3, 5, and 7 exhibit kink angles similar to those in the crystal structure, the values differ up to 6−14° when comparing the simulations performed with different lipid types. Finally, the kinks in helices 1 and 4 remain in all cases relatively unaltered and close to the values of the crystal structure.

The largest tilt for the protein as a whole observed for the bi-unsaturated PLPC lipids is in good agreement with recent results from both experiments and MD simulations that evidenced the existence of lipid specificity on rhodopsin and that suggest a tight packing of the polyunsaturated chains to the helices.[25,71] Moreover, despite recent MD simulations of model transmembrane peptides that suggest that under positive mismatch the system alleviates it predominantly by tilting the peptide and to a lower extent increasing lipid order in the vicinity of the peptide, the case of rhodopsin is different. Specifically, the system exhibiting the largest membrane−protein hydrophobic mismatch (DMPC) does not exhibit the largest tilt angles either for the protein or for the helices. This suggests a different mechanism for alleviating the positive mismatch in the case of proteins than for small peptides. It has been shown below that the polar protein residues involved in hydrogen bonds with the lipid oxygens are located on two rings on each side of the protein (see Figures 4 and 5). Roughly speaking, if we consider that both peptides and GPCRs can be approximated by cylinders, the much larger radius of rhodopsin would fail to allocate properly the ring of polar residues for large tilt angles without losing the hydrogen bonds with the lipid oxygens. On the contrary, the negligible radius of an α-helix peptide when compared to a seven-α-helix bundle membrane spanning protein such as rhodopsin allows keeping these interactions independently of the tilt angle. Thus, the results suggest that, despite that the contribution of the LJ term to the lipid−protein interactions is the largest, the electrostatic one is responsible for restraining the relative orientation of the protein to the bilayer.

Conclusions

The present work addresses the effect of lipid composition on the structural features of rhodopsin. For this purpose, four 20 ns MD trajectories of different one-component lipid bilayers were carried out. The systems included four phospholipid types with a phosphatidylcholine head and different acyl chains. Specifically, two bilayers with saturated lipids, DMPC and DPPC, and two bilayers with unsaturated lipids, POPC and PLPC, were considered for the present study.

The results show that on the one hand, lipids can modulate the structure of rhodopsin by affecting the tilt of the protein as a whole and the rigid-body motions involving helix kinks. However, the helix tilts as well as the secondary elements of the protein are not much affected by the lipidic environment, with the TM helices remaining relatively unaltered, and with only the least structured elements showing sensitivity to the lipid type. On the other hand, the protein infers an ordering effect over the lipid bilayer that depends on the difference between the equilibrium thickness of the former and the hydrophobic thickness of the latter, as can be observed in the variation of the bilayer thickness with the distance from the protein. Moreover, lipids with saturated acyl chains exhibit a poorer adaptation to the protein than lipids with unsaturated chains. Similarly, short acyl chains also exhibit an impaired matching because of the extended conformations that are forced to adopt to accommodate to the hydrophobic protein surface.

The analysis of lipid−protein interaction energies together with the study of the specific protein−lipid contacts shows differences between the systems studied. Regarding the hydrophobic interactions, the analysis of the specific lipid−protein contacts revealed that almost a third of the rhodopsin residues participate in interactions with the surrounding lipids, including amino acids phenylalanine, leucine, isoleucine, and valine which exhibit the largest number of contacts. Regarding the electrostatic contribution, the analysis of hydrogen bonds between protein donors and lipid oxygens revealed the importance of these interactions for the anchoring of the protein to the membrane. In the four systems, residues R252, K339, Y96, Y274, H152, and T108—and to a lower extent K66, R69, Y136, Y223, and W35—are found to participate in hydrogen bonds with lipid molecules and, therefore, they can be considered to be putative hooks of the protein to the bilayer. Of remarkable interest is the finding that the localization of these interactions is asymmetric regarding the two halves of the protein, suggesting that the cytoplasmic side of the protein is much more sensitive to the lipidic environment. Moreover, the analysis of salt bridges in rhodopsin revealed that lipids modulate the conformations of the cytoplasmic loops as well as the C-terminus. The results suggest a role of the lipid composition in modulating the electrostatic lock on the cytoplasmic side of helices 3 and 6.

Acknowledgment. A.C. wishes to express his gratitude to the Technical University of Catalonia for a fellowship to undertake his doctoral studies. We thank to the Biocomputing group of Dr. Peter Tieleman, at the University Of Calgary, for sharing their structure and topology files for lipids. The Spanish Ministry of Science and Technology supported this work through Grant No. SAF2005-08148-C04-01.

References and Notes

(1) White, S. H.; Wimley, W. C. *Annu. Rev. Biophys. Biomed.* **1999**, *28*, 319.
(2) Singer, S. J.; Nicolson, G. L. *Science.* **1972**, *175*, 720.
(3) Engelman, D. M. *Nature.* **2005**, *438*, 578.
(4) Jensen, M. O.; Mouritsen, O. G. *Biochim. Biophys. Acta* **2004**, *1666*, 205.
(5) Kandasamy, S. K.; Larson, R. G. *Biophys. J.* **2006**, *90*, 2326.
(6) Goodyear, D. J.; Sharpe, S.; Grant, C. W.; Morrow, M. R. *Biophys. J.* **2005**, *88*, 105.
(7) Nymeyer, H.; Woolf, T. B.; Garcia, A. E. *Proteins.* **2005**, *59*, 783.
(8) Leontiadou, H.; Mark, A. E.; Marrink, S. J. *J. Am. Chem. Soc.* **2006**, *128*, 12156.
(9) Yandek, L. E.; Pokorny, A.; Floren, A.; Knoelke, K.; Langel, U.; Almeida, P. F. *Biophys. J.* **2007**.
(10) Yeagle, P. L.; Bennett, M.; Lemaitre, V.; Watts, A. *Biochim. Biophys. Acta* **2006**.
(11) Archer, E.; Maigret, B.; Escrieut, C.; Pradayrol, L.; Fourmy, D. *Trends Pharmacol. Sci.* **2003**, *24*, 36.
(12) Ellis, C. *Nat. Rev. Drug Discovery* **2004**, *3*, 575.
(13) Attwood, T. K.; Findlay, J. B. *Protein Eng.* **1994**, *7*, 195.
(14) Palczewski, K.; Kumasaka, T.; Hori, T.; Behnke, C. A.; Motoshima, H.; Fox, B. A.; Le, Trong, I.; Teller, D. C.; Okada, T.; Stenkamp, R. E.; Yamamoto, M.; Miyano, M. *Science.* **2000**, *289*, 739.
(15) Teller, D. C.; Okada, T.; Behnke, C. A.; Palczewski, K.; Stenkamp, R. E. *Biochemistry* **2001**, *40*, 7761.
(16) Okada, T.; Fujiyoshi, Y.; Silow, M.; Navarro, J.; Landau, E. M.; Shichida, Y. *Proc. Natl. Acad. Sci. U.S.A.* **2002**, *99*, 5982.
(17) Li, J.; Edwards, P. C.; Burghammer, M.; Villa, C.; Schertler, G. F. X. *J. Mol. Biol.* **2004**, *343*, 1409.
(18) Okada, T.; Sugihara, M.; Bondar, A. N.; Elstner, M.; Entel, P.; Buss, V. *J. Mol. Biol.* **2004**, *342*, 571.
(19) Huber, T.; Botelho, A. V.; Beyer, K.; Brown, M. F. *Biophys. J.* **2004**, *86*, 2078.
(20) Crozier, P. S.; Stevens, M. J.; Forrest, L. R.; Woolf, T. B. *J. Mol. Biol.* **2003**, *333*, 493.
(21) Saam, J.; Tajkhorshid, E.; Hayashi, S.; Schulten, K. *Biophys. J.* **2002**, *83*, 3097.
(22) Lemaitre, V.; Yeagle, P.; Watts, A. *Biochemistry* **2005**, *44*, 12667.
(23) Feller, S. E.; Gawrisch, K.; Woolf, T. B. *J. Am. Chem. Soc.* **2003**, *125*, 4434.
(24) Pitman, M. C.; Grossfield, A.; Suits, F.; Feller, S. E. *J. Am. Chem. Soc.* **2005**, *127*, 4576.
(25) Grossfield, A.; Feller, S. E.; Pitman, M. C. *Proc. Natl. Acad. Sci. U.S.A.* **2006**, *103*, 4888.
(26) Berman, H. M.; Westbrook, J.; Feng, Z.; Gilliland, G.; Bhat, T. N.; Weissig, H.; Shindyalov, I. N.; Bourne, P. E. *Nucleic Acids Res.* **2000**, *28*, 235.
(27) Fahmy, K.; Jager, F.; Beck, M.; Zvyaga, T. A.; Sakmar, T. P.; Siebert, F. *Proc. Natl. Acad. Sci. U.S.A.* **1993**, *90*, 10206.
(28) Sandberg, L.; Edholm, O. *Proteins* **1999**, *36*, 474.
(29) Berendsen, H. J. C.; van der Spoel, D.; van Drunen, R. *Comput. Phys. Commun.* **1995**, *91*, 43.
(30) Lindahl, E.; Hess, B.; van der Spoel, D. *J. Mol. Model.* **2001**, *7*, 306.
(31) Lindahl, E.; Edholm, O. *Biophys. J.* **2000**, *79*, 426.
(32) Cordomi, A.; Edholm, O.; Perez, J. J. *J. Comput. Chem.* **2007**, *28*, 1017.
(33) Berendsen, H. J. C.; Postma, J. P. M.; DiNola, A.; Haak, J. R. *J. Chem. Phys.* **1984**, *81*, 3684.
(34) Miyamoto, S.; Kollman, P. A. *J. Comput. Chem.* **1992**, *13*, 952.
(35) Darden, T.; York, D.; Pedersen, L. *J. Chem. Phys.* **1993**, *98*, 10089.
(36) Jorgensen, W. L.; Maxwell, D. S.; TiradoRives, J. *J. Am. Chem. Soc.* **1996**, *118*, 11225.
(37) Berger, O.; Edholm, O.; Jähnig, F. *Biophys. J.* **1997**, *72*, 2002.
(38) Nagle, J. F.; Tristram-Nagle, S. *Biochim. Biophys. Acta* **2000**, *1469*, 159.
(39) Hofsass, C.; Lindahl, E.; Edholm, O. *Biophys. J.* **2003**, *84*, 2192.
(40) Wohlert, J.; Edholm, O. *Biophys. J.* **2004**, *87*, 2433.
(41) Bachar, M.; Brunelle, P.; Tieleman, D. P.; Rauk, A. *J. Phys. Chem. B* **2004**, *108*, 7170.
(42) Jorgensen, W. L.; Chandrasekhar, J.; Madura, J. D.; Impey, R. W.; Klein, M. L. *J. Chem. Phys.* **1983**, *79*, 926.
(43) Hayashi, S.; Tajkhorshid, E.; Schulten, K. *Biophys. J.* **2002**, *83*, 1281.
(44) Hofsäβ, C.; Lindahl, E.; Edholm, O. *Biophys. J.* **2003**, *84*, 2192.
(45) Kucerka, N.; Liu, Y. F.; Chu, N. J.; Petrache, H. I.; Tristram-Nagle, S. T.; Nagle, J. F. *Biophys. J.* **2005**, *88*, 2626.
(46) Konig, B.; Dietrich, U.; Klose, G. *Langmuir.* **1997**, *13*, 525.
(47) Mukhopadhyay, P.; Monticelli, L.; Tieleman, D. P. *Biophys. J.* **2004**, *86*, 1601.
(48) Anézo, C.; de Vries, A. H.; Holtje, H. D.; Tieleman, D. P.; Marrink, S. J. *J. Phys. Chem. B* **2003**, *107*, 9424.
(49) Böckmann, R. A.; Grubmüller, H. *Angew. Chem., Int. Ed.* **2004**, *43*, 1021.
(50) Böckmann, R. A.; Hac, A.; Heimburg, T.; Grubmüller, H. *Biophys. J.* **2003**, *85*, 1647.
(51) Pandit, S. A.; Bostick, D.; Berkowitz, M. L. *Biophys. J.* **2003**, *84*, 3743.
(52) Seelig, A.; Seelig, J. *Biochemistry* **1977**, *16*, 45.
(53) Stillwell, W.; Wassall, S. R. *Chem. Phys. Lipids* **2003**, *126*, 1.
(54) Holte, L. L.; Peter, S. A.; Sinnwell, T. M.; Gawrisch, K. *Biophys. J.* **1995**, *68*, 2396.
(55) Klein-Seetharaman, J.; Reeves, P. J.; Loewen, M. C.; Getmanova, E. V.; Chung, L.; Schwalbe, H.; Wright, P. E.; Khorana, H. G. *Proc. Natl. Acad. Sci. U.S.A.* **2002**, *99*, 3452.
(56) Deol, S. S.; Bond, P. J.; Domene, C.; Sansom, M. S. *Biophys. J.* **2004**, *87*, 3737.
(57) Bond, P. J.; Sansom, M. S. *J. Am. Chem. Soc.* **2006**, *128*, 2697.
(58) Mishra, V. K.; Palgunachari, M. N.; Segrest, J. P.; Anantharamaiah, G. M. *J. Biol. Chem.* **1994**, *269*, 7185.
(59) Saiz, L.; Bandyopadhyay, S.; Klein, M. L. *J. Phys. Chem. B* **2004**, *108*, 2608.
(60) Strandberg, E.; Killian, J. A. *FEBS Lett.* **2003**, *544*, 69.
(61) Tieleman, D. P.; Forrest, L. R.; Sansom, M. S.; Berendsen, H. J. *Biochemistry* **1998**, *37*, 17554.
(62) Grossfield, A.; Woolf, T. B. *Langmuir* **2002**, *18*, 198.
(63) Faraldo-Gomez, J. D.; Forrest, L. R.; Baaden, M.; Bond, P. J.; Domene, C.; Patargias, G.; Cuthbertson, J.; Sansom, M. S. *Proteins* **2004**, *57*, 783.
(64) Grossfield, A.; Feller, S. E.; Pitman, M. C. *Proteins* **2007**, *67*, 31.
(65) Ballesteros, J. A.; Shi, L.; Javitch, J. A. *Mol. Pharmacol.* **2001**, *60*, 1.
(66) Crocker, E.; Eilers, M.; Ahuja, S.; Hornak, V.; Hirshfeld, A.; Sheves, M.; Smith, S. O. *J. Mol. Biol.* **2006**, *357*, 163.
(67) Ballesteros, J. A.; Jensen, A. D.; Liapakis, G.; Rasmussen, S. G.; Shi, L.; Gether, U.; Javitch, J. A. *J. Biol. Chem.* **2001**, *276*, 29171.
(68) Killian, J. A. *FEBS Lett.* **2003**, *555*, 134.
(69) Lee, A. G. *Biochim. Biophys. Acta* **2003**, *1612*, 1.
(70) Venturoli, D.; Rippe, B. *Am. J. Physiol.: Renal* **2005**, *288*, F605.
(71) Soubias, O.; Teague, W. E.; Gawrisch, K. *J. Biol. Chem.* **2006**, *281*, 33233.